参考著作No.14


ASCE LIBRARY
SEARCH
CART
LOG IN / REGISTER
JOURNALS
BOOKS
MAGAZINE
AUTHOR SERVICES
USER SERVICES
Journal of Performance of Constructed Facilities / Volume 32 Issue 1 - February 2018
Technical Papers
Downloaded 235 times
DETAILS
FIGURES
REFERENCES
RELATED
Reliability-Based Design Optimization of a River Bridge Considering Uncertainty in Scours
Kuo-Wei Liao; Wei-Lun Chen; and Bang-Ho Wu
FULL TEXT
DOWNLOAD
TOOLS
SHARE
Authors
Kuo-Wei Liao
Associate Professor, Dept. of Bioenvironmental Systems Engineering, National Taiwan Univ., No. 1, Section 4, Roosevelt Rd., Taipei 10617, Taiwan (corresponding author). E-mail: kliao@ntu.edu.tw

Reliability-Based Design Optimization of a River Bridge Considering Uncertainty in Scours

Kuo-Wei Liao[1]; Wei-Lun Chen[2]; and Bang-Ho Wu[3]

Abstract: Safety assessments of river bridges have attracted a great deal of attention from researchers. Regardless of whether a bridge is being constructed or retrofitted, an integrated analysis of many factors, such as hydraulic conditions, geological conditions, and structural strength, is necessary. A three-dimensional finite-element model is used here to perform structural analysis. The uncertainty in important parameters (such as water level, water flow rate, scouring depth, and the *N* value of the standard penetration test) was considered via a reliability analysis. A parameterized bridge model was established to perform the iterative calculations required for the optimization and reliability analysis, in which the preprocessing, solution, and postprocessing were all performed automatically to facilitate a reliability-based optimization. To reduce the number of calculations, a surrogate model was adopted, in which the reliability analysis uses the first-order second-moment method and the optimization uses the particle swarm optimization method. A numerical example (the Dongshi Bridge) is given to demonstrate the methodologies proposed in the study. **DOI: 10.1061/(ASCE)CF.1943-5509.0001118.**

Author keywords: Particle swarm optimization; Optimum; Successful probability; Bridge foundation; First-order second-moment.

Introduction

River bridges play an essential role in Taiwan's transportation network. Taiwan's geographic characteristics of elongation in the northern and southern directions with mountains rising in the central regions cause the rivers in the east and west to flow at high speeds such that riverbeds are eroded and the foundations of bridges are likely to be scoured. In recent years, multiple bridge disasters have occurred. For example, Typhoon Bilis caused the Kaoping Bridge to collapse without warning in 2000 (Liao et al. 2016); Typhoon Sinlaku caused damage to four bridges, the Hofeng Bridge, the Jiasian Bridge, the Nioumian Bridge, and the Wuhuliao Bridge, in 2008 due to flood impacts; and Typhoon Morakot caused more than 60 bridges throughout Taiwan, including the Shuangyuan Bridge (NCDR 2010), to be damaged by floods in 2009. Prior to these bridge damage events, riverbed erosion commonly pre-existed in these areas; therefore, the occurrence of scouring has a significant impact on the overall safety of bridges and has gained great attention from researchers (Ni et al. 2012; Ko et al. 2014; Lin et al. 2015). Wardhana and Hadipriono (2003) investigated 500 bridge structure failures in the United States between 1989 and 2000. They found that bridge failures could be attributed most frequently to hydraulic causes. For example, flooding and scouring were the leading causes of bridge failures (48.31% of the total). Note that there were close to 20 failure causes investigated; besides flood, scour, and collision (11.73% of the total), none of the other causes had a failure percentage greater than 10%. That is, flooding and scouring were the most dominant factors. Despite the lack of official statistical data concerning the causes of bridge failures in Taiwan, it is commonly recognized that the situation in Taiwan is likely to have the same trends as that in the United States. Therefore, the aim of this study is to evaluate bridge safety against floods. In addition, conventional bridge safety assessments primarily focus on analyses, whereas design often attracts relatively less attention. However, if various uncertain factors can be taken into consideration during the design stage to propose an optimized design, it could be possible to reduce safety concerns over a bridge's service life. Therefore, developing an efficient and practical reliability-based design optimization (RBDO) algorithm for a river bridge is an additional focus of this study.

Uncertainties in a bridge's analysis/design are often inevitable. It is common to use a deterministic analysis with a safety factor to take these uncertainties into consideration. The safety factor approach, however, cannot identify which design parameters are more critical because all the uncertainties are represented by a single factor throughout the design. Conversely, RBDO incorporates a probabilistic analysis with an optimization technique to find the best design within a feasible domain. The major drawback of RBDO is its computational cost, which is often high compared to that of deterministic analyses. The heavy computation cost is primarily due to the reliability analysis performed inside the optimization loop. To lessen this computational burden, several RBDO algorithms have been proposed (Aoues and Chateauneuf 2010; Li et al. 2010; Liao and Lu 2012; Liang et al. 2007; Kaymaz and Marti 2007; Shan and Wang 2008; Motta and Afonso 2016); the current study used the least-square support vector machine (LS-SVM) (Suykens et al. 2002) method to build a surrogate model representing the relationship between the influencing factors and the reliability index (β), in which the β value was computed using the first-order second-moment (FOSM) method. The particle swarm optimization (PSO) algorithm was used as an optimizer to find the appropriate bridge dimensions. Several common indices were used

[1]Associate Professor, Dept. of Bioenvironmental Systems Engineering, National Taiwan Univ., No. 1, Section 4, Roosevelt Rd., Taipei 10617, Taiwan (corresponding author). E-mail: kliao@ntu.edu.tw

[2]Junior Engineer, Jianbao Construction Co., No. 48, Zhongrong Ln., Nantun District, Taichung City 40859, Taiwan. E-mail: calendulamg@hotmail.com

[3]Project Engineer, Moh and Associates Inc., Oriental Technopolis Bldg. A, 22 Floor, No. 112, Xintai Wu Rd., Section 1, Xizhi District, New Taipei City 22102, Taiwan. E-mail: vbhdgtj56953@gmail.com

Note. This manuscript was submitted on October 26, 2016; approved on July 12, 2017; published online on November 13, 2017. Discussion period open until April 13, 2018; separate discussions must be submitted for individual papers. This paper is part of the ***Journal of Performance of Constructed Facilities***, © ASCE, ISSN 0887-3828.

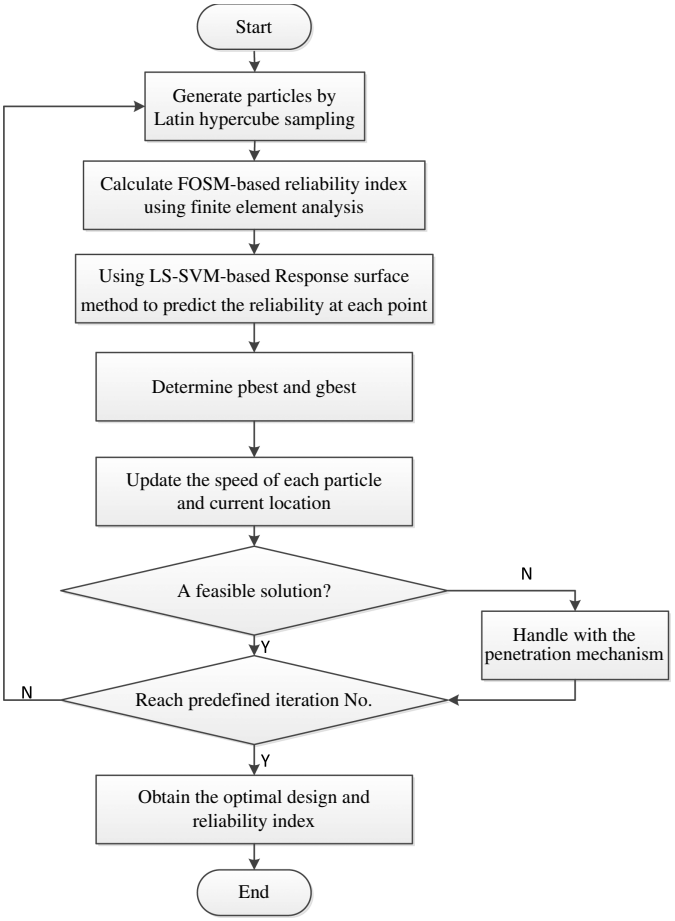

Fig. 1. Flowchart of RBDO algorithm used in this study

to ensure the accuracy of the surrogate model built by the LS-SVM method. In addition, a parameterized *ABAQUS* model was established to facilitate the process of reliability analysis and the optimization calculations. Fig. 1 displays the calculation flowchart of the proposed RBDO algorithm. As shown in Fig. 1, to take advantage of existing software (i.e., *ABAQUS*), a computational framework for recursive analyses, which is a necessary process in reliability analysis and optimization, was established using the scripting language Python. The framework integrates the commercial finite-element software, reliability analysis, optimization, and the surrogate model to carry out a structural reliability-based design optimization. As shown in Fig. 1, two interim optimums are required to obtain the final optimal solution: *pBest* and *gBest*. The *pBest* optimum refers to the particle position with the minimum objective value in its own population and *gBest* refers to the particle position with the minimum objective value in the entire population. Details of the proposed algorithm are described subsequently, followed by a bridge example.

Establishing the Parameterized *ABAQUS* Model

The target structure of this study is a river bridge with a single-pier piled foundation. Six types of pile arrangements are considered: 3×3, 4×2, 4×3, 4×4, 5×4, and 5×5. The original arrangement (i.e., 3×3) was selected as the baseline design, which is often the lower bound among the considered arrangements. On the other hand, the arrangement of 5×5 is the upper bound design. There are many possible designs between the lower and upper bounds, including pile arrangements such as $N \times M$ or $M \times N$ (N = number of piles in river direction, M = number of piles in road direction). To save computational cost, only four additional arrangements, which are often found in practice, were selected for analysis. The parameterized variables in the finite-element model are shown in Table 1. In Table 1, the variables can generally be divided further into two types of geometric-related and material-related variables, which include a total of 22 parameterized variables.

The finite-element model used in this study is based on the following assumptions:

1. The boundary of the soil model is fixed.
2. Steel bars are simulated using beam elements and are arranged at the surface of the pier; that is, the strength of the concrete cover is ignored. Such settings facilitate meshing the pier and connecting the pier cap and pile cap without significantly influencing the structural analysis.

Element Type

A three-dimensional, eight-node element (C3D8) was used for the bridge and column and a three-dimensional, 10-node element (C3D10) was used for the pier cap and pile cap, as shown in Fig. 2. The pier cap (or pile cap) was connected to the circular pier such that its geometric relationship was more complicated: If C3D8 is used in the cap area, the automatic meshing may be subject to analysis precision problems and overly long analysis times. Consequently, C3D10 was used instead of C3D8 to increase the likelihood of success with the automatic model construction.

Soil Column Settings of Numerical Analysis Model

The parameters of the soil column refer to the dimensions of the column, the number of soil layers, and the material properties of each layer. The following describes the setting methods:

1. The horizontal dimensions of the soil. This dimension is often expressed using kD (Fu 2012), where D is the distance between the outermost piles (Fig. 3) and k is a multiplier larger than 1. Primary factors used to determine the value of k include the computing cost and the desired precision. Under the assumption of having similar displacement with Chang's formula, via trial and error, the value of k determined for this study was 10. Because this study only considers the horizontal forces induced by floods and ignores the settlement effect caused by vertical loads, unlike in the case of the horizontal dimension, the effect of the vertical dimension of the soil was not investigated. A length

Table 1. Parameterized Variables in Finite-Element Model

Parameter type	Parameter name
Geometric-related	Pier diameter, pier depth, pile cap depth, pile cap width, pile cap length, pile diameter, pile depth, pile group arrangement, total depth of soil, scour depth, water level, water velocity, number of soil layers, thickness of each individual soil layer, diameter of steel bar
Material-related	Elastic modulus and Poisson ratio of concrete, elastic modulus and Poisson ratio of steel, elastic modulus and Poisson ratio of each individual soil layer

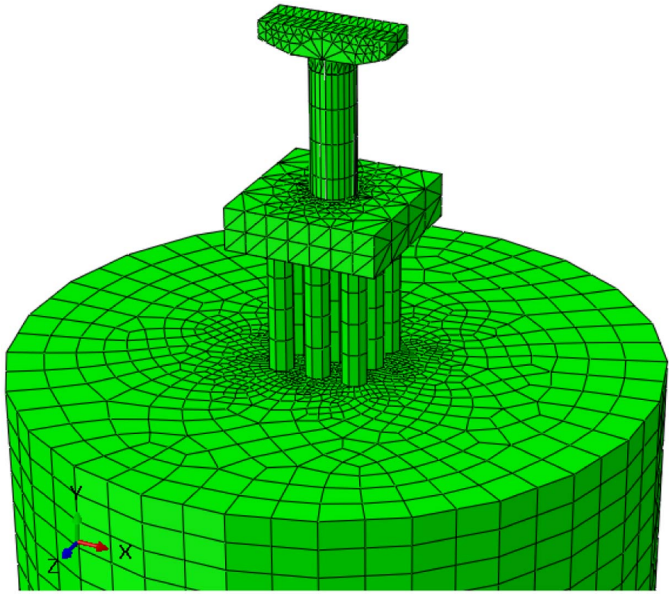

Fig. 2. Meshing diagram of three-dimensional model

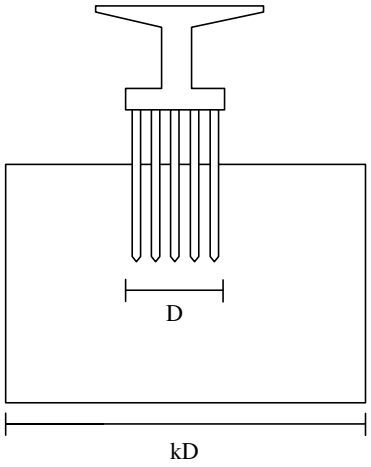

Fig. 3. Concept diagram for three-dimensional soil diagram

greater than the pile embedded length was used for the vertical soil length in the model.

2. The number of soil layers. Drilling reports provided in the design drawing were used to determine the soil properties and the number of soil layers. Based on the survey, the maximum number of soil layers that can be accommodated within the parameterized *ABAQUS* model is six.
3. The Poisson's ratios of the soils used here are listed in Table 2.
4. The stability of a bridge was selected as the deterministic analysis in the current study, in which five limit states were considered. Such a procedure is often used as a preliminary safety evaluation in Taiwan and is often considered a relatively conservative analysis. Thus, the material response often remains in the elastic stage. For this reason, the linear model is used for concrete and the perfect bilinear model is used for steel and soil. The yield stress and passive stress are the transition points for steel and soil, respectively. Mesh size depends on several factors, such as accuracy, cost, and automatic meshing. In consideration of the aforementioned factors, the mesh size was arranged in a range from 100 to 200 cm.

Table 2. Poisson's Ratios of Soil Layers

Soil type	Poisson's ratio
Clay	0.35
Sand	0.3
Gravel	0.25

Process Flow Using Python to Establish Automatic Design

In this study, the Python script provided by *ABAQUS* was used to modify the parameters to achieve automatic model construction. The following briefly describes the steps of model construction:

1. For the process, divide the three-dimensional model into two major parts: the bridge body and the soil column.
2. Select the type of foundation pile.
3. Use three-dimensional coordinates to perform the model construction, and replace these coordinates with variables.
4. Once the bridge body shape is completely constructed, use a planar method to determine the locations where forces are applied by the water pressure.
5. The soil column construction process is similar to that of the bridge body; use the planar method to determine the number of soil layers and the thicknesses required.
6. Use the beam element to simulate the steel bars in the pier.
7. Assemble the bridge body, steel bar, and soil column.
8. Set up the external forces and boundary conditions.
8. Set up the element type for each portion.
9. Use the seed part method to complete the meshing.
10. Merge the bridge body, steel bar, and soil column based on the grid.
11. Perform a finite-element analysis.
12. Repeat the previous steps to complete the constructions for all six types of foundation pile types.

Soil Column Verification of Numerical Analysis Model

Because the soil properties exert critical influences on the analytical results, the soil model used here was verified as follows. Because the design specifications in Taiwan allow engineers to use the Y-L Chang lateral pile analysis method to compute the response of the soil, this method was used for verification in this study. Chang and Chou (1989) categorized the pile foundations into six types depending on their boundary conditions. Based on each category, the pile shear stress, the pile axial stress, and the horizontal displacement on the pile head can be calculated. For example, if the pile cap is categorized as a fixed end, the pile head displacement can be computed as follows:

$$\text{displ.} = 0.01\left(\frac{V_t}{2EI\lambda^3} + \frac{M_t}{2EI\lambda^2}\right) \tag{1}$$

where V_t = applied shear force on top of pile (tf); $\lambda = \sqrt[4]{kD/EI}$ (m^{-1}); k = horizontal subgrade reaction coefficient (tf/m^3); D = pile diameter (m); E = elastic modulus (tf/m^2); I = pile cross-sectional moment of inertia (m^4); and M_t = applied bending moment on pile head. To comply with the analytic mode of such an analysis method, an additional single-pile model was constructed, with identical boundary condition settings to the ones previously described. Table 3 shows the parameters used in the analysis, in which the horizontal dimensions of the soil include four dimensions for the simulations (Table 4). The verification results are shown in Table 4 and Fig. 4. From the table and figure, it can be seen that the most preferable soil size is 10D with a margin

Table 3. Parameter Settings of Single-Pile Analysis Model

Soil parameter	Setting value	Units
Outermost foundation pile distance (D)	0.1	m
Concrete compression strength ($f'c$)	21	MPa
Pile buried depth	2	m
Soil type	Sand	N/A
Soil penetration N value	20	N/A
Poisson's ratio of the soil	0.3	N/A
Horizontal subgrade reaction coefficient	4.8×10^{-5}	N/m^3
Soil elastic modulus	14.4	MPa
Horizontal force of pile top	1.5×10^6	N

Table 4. Comparison of Pile Top Displacements of Soil Layers with Different Diameters

Soil diameter multiples (k)	Theoretical value (Chang)	Simulated value (*ABAQUS*)	Error (%)
5	1.018	0.935	8.13
10	1.018	1.076	5.72
20	1.018	1.132	11.22
40	1.018	1.292	26.94

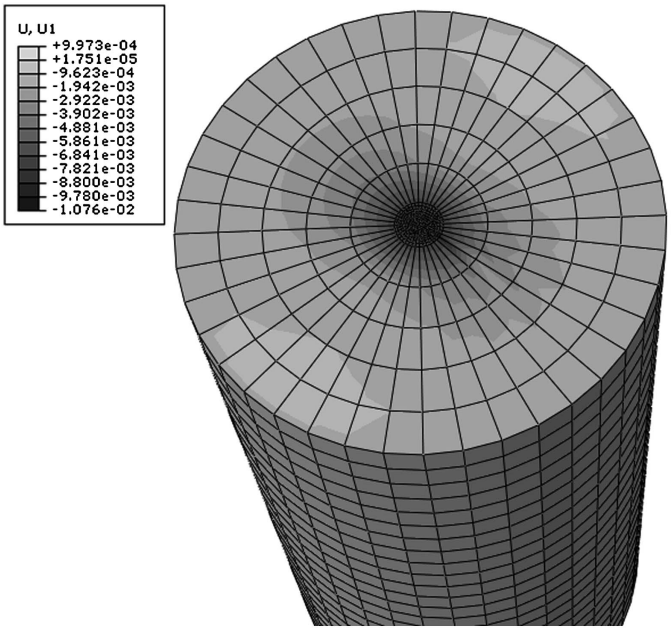

Fig. 4. Single-pile simulation analysis result—displacement (using the dimension of 10D as an example)

of error of approximately 5.72%. Therefore, in this study, 10D was selected as the horizontal dimension for the soil model.

Random Variables and Reliability Analysis

For the time-independent reliability analysis, the failure probability of a given design can be written as Eq. (2)

$$p_f = \int \cdots \int_D f_X(x)dx \tag{2}$$

where $f_X()$ = probability distribution function (PDF) in $\boldsymbol{X}$, which is the vector of the basic variables in n-space. The *failure domain* D is defined by one or more constraint functions, $G_i(\boldsymbol{X}) \leq 0$, $i = 1, 2, \ldots, m$. The integral in Eq. (2) is generally very complicated to calculate. Approximate methods to estimate the failure probability have been proposed, including first-order reliability method (FORM) analysis and Monte Carlo simulations (MCSs). The FORM technique computes the failure probability via an optimization procedure. The objective is to minimize the distance between the origin and the most probable point (MPP) in the reduced space, with the constraint that the MPP must be on the limit state function. The obtained distance is called the reliability index (β), and the failure probability can be easily calculated from β. In MCS, a simulation approach, the basic variables are generated based on their PDFs and the limit state function is repeatedly evaluated using the generated variables. If the failure probability is very small, a large sample size is often required for the MCS approach.

This study considers five limit state functions corresponding to the performances of pile shear stress, pile axial stress, bridge serviceability (the horizontal displacement on the pile head), soil bearing, and soil pulling force. The FOSM method was selected for the reliability analysis. Because the deterministic analysis (i.e., the *ABAQUS* analysis) used here induces an implicit limit state function, a first-order Taylor series was used to approximate the limit state function in which the mean values of the random variables are the expansion points. The constructed Taylor series [e.g., $g(\boldsymbol{X})$] was used to acquire both μ_g and σ_g [the mean value and standard deviation indicated in Eqs. (3) and (4)], which are necessary parameters to calculate the FOSM-based reliability index, as described in Eq. (5)

$$\mu_g = -\sum_{i=1}^{n} \mu_{X_i'} \left(\frac{\partial g}{\partial X_i'} \right) \tag{3}$$

$$\sigma_g^2 = \sum_{i=1}^{n} \sigma_{X_i}^2 \left(\frac{\partial g}{\partial X_i} \right) = \sum_{i=1}^{n} \left(\frac{\partial g}{\partial X_i'} \right) \tag{4}$$

$$\beta = \frac{\mu_g}{\sigma_g} \tag{5}$$

where $\boldsymbol{X}'$ = random variable in standard space; and $\mu_{X_i'}$ = mean value for each random variable. The resulting β can be converted into the corresponding reliability (ρ), as shown in Eq. (6)

$$\rho = \Phi(\beta) \tag{6}$$

where Φ = cumulative probability density function of the standard normal distribution. As shown, a greater distance (β) will lead to a higher reliability (ρ) and vice versa.

A total of three random variables were considered during the reliability analysis: water level, stream velocity, and scouring depth. Detailed information concerning these random variables is described subsequently.

Stream Velocity and Water Level

Currently, the mean values of stream velocity and water levels corresponding to the 100-year returning period are used for bridge design in Taiwan (Liao et al. 2015). This helps engineers simplify the design procedure. However, reliability analysis needs more information, such as variation in stream velocity and the corresponding PDF. This study therefore utilizes the Hydrologic Engineering Center's River Analysis System (HEC-RAS) with relevant hydrological data (such as upstream flow volume and Manning's coefficient), mainly collected from the Geographical Information Center of the Water Resources Agency of the Ministry of Economic

Table 5. Statistics of Random Variables Considered in This Study

Random variable	Average value	Standard deviation
Scouring depth	7.62 m	5.57
Water level	4.91 m	1.56
Water flow rate	6.50 m/s	1.77
Manning coefficient	0.02–0.045	—
Elastic modulus for $N = 100$	30,900 MPa	8,157.8

Affairs (MOEA) as well as the reports of regulation planning for various river basins, to establish a probabilistic-based hydraulic model. That is, the stream velocity and water level are obtained via Monte Carlo simulation. Once the execution number reaches the predefined target value (i.e., 30), the coefficient of variation (COV) and PDF for stream velocity and water level can be readily computed. The statistics are summarized in Table 5. Note that the Manning coefficient in the HEC-RAS model is a random variable and its values vary depending on bridge location. The HEC-RAS model allows the user to perform one-dimensional steady flow calculations, one-dimensional and two-dimensional unsteady flow calculations, sediment transport/mobile bed computations, and water temperature/water quality modeling (ACE/HEC 1997).

Calculating Local Scouring Depths

Together with other parameters, such as pier width and riverbed properties, calculated water level and stream velocity are used to compute the local scouring depth for each bridge using the empirical formulae suggested by Liao et al. (2015). The information needed for the scouring depth in the reliability analysis is mean value, standard deviation, and PDF. The average of the results for each empirical equation is the mean value of the scouring depth. The standard deviation for the scouring depth is one-sixth the difference between the minimum and maximum values obtained from each empirical equation. The PDF is determined via the chi-square test using the results of the empirical formulae. Note that the stream velocity, water level, and local scouring depth used in this study were either directly or indirectly acquired from the hydraulic analysis. These three variables are therefore highly correlated (with a correlation coefficient of 0.9 or above). Table 5 shows the calculation results of the random variables for the selected bridges. The scouring depth exhibited a relatively high variance (with a COV of 0.73).

Reliability Analysis Using Response Surface

Computationally, FOSM is a relatively efficient method compared to other types of reliability analyses; however, because finite-element analysis is used in this study, it is extremely time-consuming. As a result, in addition to the use of FOSM, response surface methodology (RSM) was used to increase the computational efficiency of the reliability analysis method. The purpose of RSM is to establish a relationship between the design variables and the target equations to replace the original complicated relationship. Therefore, the response surface typically simplifies the characteristics of the original model and reduces analysis time. The response surface can be used to perform optimization, reliability analysis, or other analyses. The simplest method is to construct the response surface based on the polynomial method. If the design variables are $X_1, X_2, \ldots, X_n$, then the response surface (y) can be expressed as follows:

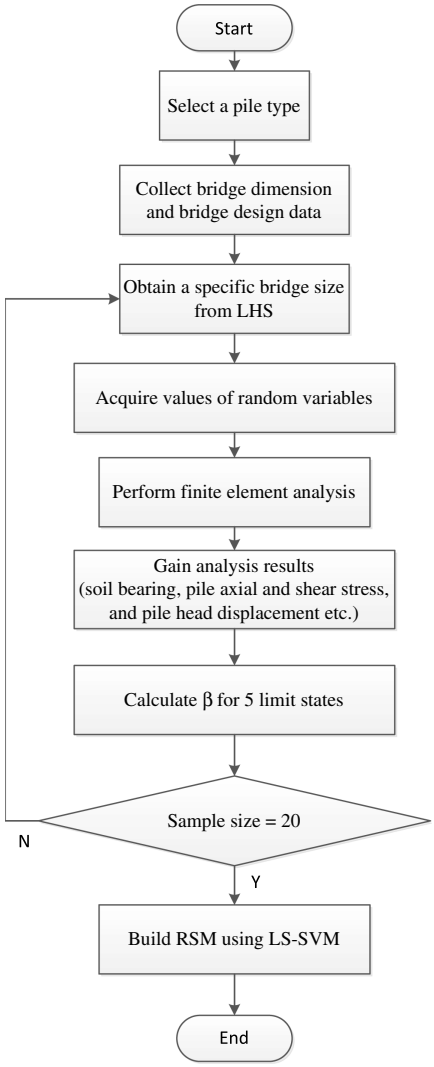

Fig. 5. Flowchart using response surface to perform reliability analysis

$$y = f(X_1, X_2, \ldots, X_n) + \varepsilon$$
$$y = \beta_0 + \sum_{i=1}^{n} \beta_i X_i + \sum_{j=1}^{n} \beta_j X_i^2 + \cdots + \varepsilon \quad (7)$$

where f refers to the original model; β_i (β_j) refers to the polynomial coefficient; and ε refers to the error and can typically be estimated using the least-squares method. The polynomial response surface clearly defines the mathematical equation and allows observations of the changes and local optimal points of the surface. However, in a situation in which the relationship between the design variables and the target output is more complicated, the polynomial response generally cannot satisfy the desired precision requirement. As a result, the LS-SVM method is used to establish the response curve. The flowchart of this method is displayed in Fig. 5. The design variables of the proposed RSM include the pier stud diameter, pier stud depth, pile cap depth, foundation pile diameter, foundation pile depth, and number of foundation piles. The output parameters include the reliability index (β) for the pile shear stress, pile axial stress, horizontal displacement on the pile head, soil bearing, and soil pulling force.

A standard SVM (Cortes and Vapnik 1995), as described in Eq. (8), solves a nonlinear classification problem by means of convex quadratic programs (QPs)

$$\underset{w,b,\xi}{\text{minimize}}\frac{1}{2}w^T w + c\sum_{k=1}^{N}\xi_k$$
$$\text{Subject to}\begin{cases} y_k(w^T K(x_i)+b) \geq 1-\xi_k \\ \xi_k \geq 0, i=1,2,\ldots,N \end{cases} \quad (8)$$

where w = normal vector to the hyperplane; c = real positive constant; ξ_k = slack variable, for which if $\xi_k > 1$, the kth inequality becomes violated compared to the inequality from the linearly separable case; y_k = class (e.g., failure or safe class); $[w^T K(x_i)+b]$ = classifier; N = number of data points; and K = kernel function. In the current study, the Gaussian radial basis function (RBF) kernel is used, as shown in Eq. (9)

$$K(X, X_i) = e^{-\sigma(||X-X_i||)^2} \quad (9)$$

where X = input vector; σ = kernel function parameter; and X_i = support vectors.

The LS-SVM method (Suykens et al. 2002), instead of solving the QP problem, solves a set of linear equations by modifying the standard SVM, as described in Eq. (10)

$$\min\frac{1}{2}w^T w + \frac{\gamma}{2}\sum_{k=1}^{N}e_k^2$$
$$\text{s.t. } y_k(w\cdot K(x_k)+b) = 1-e_k, \quad k=1,\ldots,n \quad (10)$$

where γ = constant number; and e = error variable. Compared to the standard SVM, there are two modifications leading to solving a set of linear equations. First, instead of inequality constraints, the LS-SVM uses equality constraints. Second, the error variable is a squared loss function. In this research, during the evaluation of the RSM precision, three types of indices, R^2, mean absolute percentage error (MAPE), and root mean squared error (RMSE), are used.

Reliability-Based Optimization

A general formulation of a RBDO model is described by Eq. (11), where f = design objective; $\mathbf{D}$ = design variable vector; $\mathbf{P}$ = random design variable vector representing uncertainty in design variables; $\mathbf{X}$ = random design parameter vector; $Prob.$ = probability; $G_i = i$th constraint function; α_i = reliability requirement for ith constraint; and m = number of constraints

$$\text{Min:} f(\boldsymbol{D},\boldsymbol{P},\boldsymbol{X})$$
$$\text{s.t.:} Prob.\{G_i(\boldsymbol{D},\boldsymbol{P},\boldsymbol{X}) \leq 0\} \leq \alpha_i, \quad i=1,2,\ldots,m \quad (11)$$

As shown in Eq. (11), a typical RBDO has a nested double-loop approach, in which the outer loop conducts the optimization and the inner loop considers the probabilistic analysis.

The reliability analysis used here was introduced in the section "Reliability Analysis Using Response Surface." For the optimization, this study uses PSO to find the optimal design. The PSO technique was proposed by Eberhart and Kennedy (Eberhart and Kennedy 1995; Kennedy and Eberhart 1995). An algorithm operating on the basis of a large population of solutions, PSO is currently popular because it is simple and easy to adopt. To execute a PSO, a group of random numbers is used to initialize the entire population. A population is a set of individual particles. The usual size of a population is between 20 and 30. Particle movements are influenced by the optimal experience of an individual particle and that of the population. Weighted values are used to determine the degree of influence between the two. Random elements are also considered when determining the directions of the particle movements, giving particles a chance to leave local trends and preventing them from being trapped within local optimums. Many variations have been proposed for PSOs. The following briefly describes the PSO used in this study. A new particle, which represents a set of weights in the current study, was generated using Eq. (12), as follows:

$$\vec{x}_i(t+1) = \vec{v}_i(t+1) + \vec{x}_i(t) \quad (12)$$

where $\vec{x}_i(t+1)$ denotes the position of the ith particle in the next iteration; $\vec{x}_i(t)$ denotes the position of the ith particle in the current iteration; and $\vec{v}_i(t+1)$ denotes the velocity of the ith particle in the current iteration. The position of a particle represents the values of that particle. The velocity of the ith particle is determined by Eq. (13)

$$\vec{v}_i(t+1) = w\times\vec{v}_i(t) + r_1c_1[\vec{x}_{pBest}-\vec{x}_i(t)] + r_2c_2[\vec{x}_{gBest}-\vec{x}_i(t)] \quad (13)$$

where w = inertia factor; $\vec{v}_i(t)$ = velocity at previous iteration; r_i $(i=1, 2)$ = random numbers between 0 and 1; and c_1 and c_2 = cognition and social factors, respectively. The term $\vec{x}_{pBest}$ is the particle position with the minimum objective value in the ith population and $\vec{x}_{gBest}$ is the particle position with the minimum objective value in the entire population. Detailed information concerning the PSO parameter settings can be found in Table 10. Note that each particle represents a set of design variables. In other words, a particle is a vector with a length of six, as indicated in the section "Parameter Settings of Response Surface." As mentioned previously, PSO continuously updates the location of each particle, and sometimes particles may move too fast, therefore falling into an infeasible domain. Typically, there are three ways to handle such phenomena: (1) fix the particles falling outside the feasible domain onto the search boundary; (2) maintain the inertia of the particles and enter them into the feasible domain from the opposite boundary—if such a particle is currently located outside the maximum value, it would then appear at the boundary of the minimum value; and (3) after subtracting the portion absorbed by the boundary from the particle energy, use the remaining energy to bounce the particle back into the feasible domain based on the law of reflection. In this study, the second method was used to solve the problem of the boundary value. The first method may reduce the chance of finding the global optimum. If the local optimum happens to be on the boundary, it would cause the particles to approach the boundary value, which would slow the convergence of the global optimum search. In addition, because constraints are functions of design variables, the feasible domain is continuously revised during optimization. That is, constraints at each step are different and are constructed using the design variables specified at each step.

Numerical Example and Discussion

The Dongshi Bridge, located in the midstream of the Dajia River, was used to verify the proposed optimization algorithm. The Dongshi Bridge is an important river bridge connecting the Dongshi District and the Shihgang District. Its entire length is 573 m with 22 spans; each span measures approximately 26 m. The concrete strength is 28 and 21 MPa for the bridge pier and pile, respectively. For diameters less than or equal to 16 mm, SD280 steel bars are used, whereas SD420W bars are used for diameters greater than 16 mm. The analysis process is based on the following two assumptions:

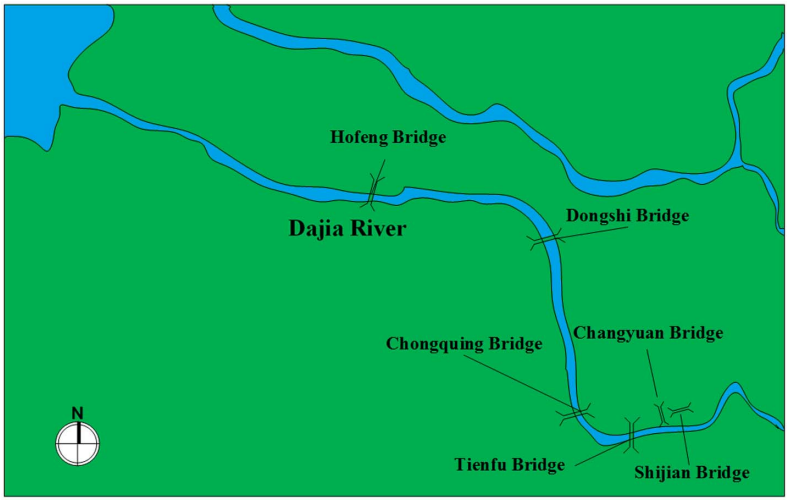

Fig. 6. Relative location map of Dongshi Bridge and drilled holes for obtained drilling data

1. The Dongshi Bridge uses double-column piers as its foundation; however, single-column piers are used as a basis for the simulations in this study. Such an assumption is based on the consideration that the limit state function does not include the failure of piers, and the external forces in this study primarily result from floods. If the influence of the angle of attack of the water flow is ignored and the space between two piers is small, the water-projected area of the hydrodynamic pressure of a double-column type pier and a single-column type pier are similar.
2. Because the drilling report of the Dongshi Bridge was unavailable, the actual soil layer conditions could not be precisely known. Consequently, other documents were used to understand the geological conditions in the midstream area of the Dajia River (Ho-Hsien Engineering and Technology Consultants 2011). From Fig. 6, it can be seen that, in addition to the Dongshi Bridge, there are five other bridges in the midstream area of the Dajia River: the Hofeng Bridge, the Chongquing Bridge, the Tienfu Bridge, the Changyuan Bridge, and the Shijian Bridge. The drilling reports for these five bridges are shown in Table 6 and indicate that the N values of the standard penetration test (SPT-N) at the midstream of the Dajia River are all nearly equivalent to 100, which means that the soil layer consists of gravel or bedrock (e.g., shale and sandstone). In addition, it is known that the stratum of the Taichung Basin consists primarily of sandstone, shale, or gravel and sandy shale dating from the Miocene to the third century Pleiocene with parts dating from the fourth century Eo-Pleistocene. According to these data, the stratum of the Dongshi Bridge primarily consists of gravel or sandy shale; therefore, the average values of the drilling data for these five bridges were used as the geological data for the Dongshi Bridge, as shown in Table 6.

Table 6. SPT-N Values for Midstream Area of Dajia River

	Bridge name					
Drilling depth	Hofeng Bridge	Chongquing Bridge	Tienfu Bridge	Changyuan Bridge	Shijian Bridge	Dongshi Bridge
1.3	100	30	46	11	22	40[a]
2.8	100	100	100	100	100	100
4.3	100	100	100	100	100	100
5.8	100	100	100	100	100	100
7.3	100	100	100	100	100	100
8.8	100	100	100	100	100	100
10.3	100	100	100	100	100	100

[a]Rounded off from 41.8.

Parameter Settings of Response Surface

In this study, Latin hypercube sampling (LHS) was used to generate samples to construct the response surface of the surrogate model. Each type of foundation pile dimension had 20 entries, and there were a total of 120 sample entries for the six dimensions. The range of each parameter was between 0.5 and 1.5 times the current dimension of the Dongshi Bridge. The settings of the LHS input parameters are shown in Table 7.

Random Variables, Material Properties, Optimization Parameters, and RBDO Formulation

The random variables considered in this study are shown in Table 5. As mentioned, the SPT-N values for the midstream section of the Dajia River are relatively stable; however, according to Pan (2007), the elastic moduli of gravel, shale, and sandstone, as shown in Table 8, vary significantly from each other; therefore, the elastic modulus is considered to be a random variable to reflect the complex geological characteristics in this area. Note that because the N

Table 7. Range of LHS Input Parameter Values

Design variable	Lower bound	Upper bound	Original dimensions
Pier diameter (m)	1.30	3.90	2.60
Pier depth (m)	4.00	12.00	8.00
Pile cap thickness (m)	1.25	3.75	2.50
Pile diameter (m)	0.75	2.25	1.50
Pile depth (m)	10.00	30.00	20.00
Number of piles	$3 \times 3 \sim 5 \times 5$		3×3

Table 8. Possible Elastic Modulus Values for $N = 100$

Soil type and statistics	Elastic modulus for $N = 100$ (MPa)
Gravel	19,000
Sandstone	32,000–41,000
Shale	28,000–34,500
Average value	30,900
Standard deviation	8,157.8

Table 9. Material Properties Used in This Study

Material type	Elastic modulus (MPa)	Poisson's ratio
Concrete (3,000 psi)	21,737	0.15
Steel bar (SD280)	230,000	0.27

Table 10. PSO Parameter Settings

Parameter	Setting value
Velocity weight (w)	0.9 decreases to 0.2
Particle weight (c1, c2)	2
Particles	100
Optimization termination	Iteration = 1,000 or convergence for 333 successive iterations[a]
Area optimization handling mechanism	Hunger mechanism
Handling mechanism for particles moving toward the boundary	Penetration mechanism

[a]Convergence means the variation between two consecutive solutions is less than 1%.

value varied significantly in the literature, both lower and upper bounds of sandstone and shale were used in the calculation of average value. The material properties of the Dongshi Bridge are shown in Table 9. The parameter settings for the PSO are shown in Table 10. The RBDO formulation is expressed by Eq. (14)

$$\text{Min:} f(\boldsymbol{D}) \qquad \text{s.t.:} Prob.\{G_i(\boldsymbol{D}, \boldsymbol{X}) \le 0\} \le \alpha_i, \quad i = 1, 2, \ldots, m \tag{14}$$

where f refers to total volume of the bridge; $\boldsymbol{D}$ refers to design variable, which includes pier diameter, pier height, pile cap thickness, pile diameter, pile depth, and foundation pile type; $\boldsymbol{X}$ refers to random variables, which include scouring depth, water level, water flow rate, Manning coefficient, and elastic modulus of the soil; and α refers to reliability requirement, which is set to 0.00315.

Analysis Results

Fig. 7 shows the finite-element *ABAQUS* model of the RBDO result, and Fig. 8 shows the displacement distribution of the optimal design.

Based on the results of RBDO as shown in Table 11, the following key points can be stated:

1. The optimization obtained from RBDO is similar to the dimensions of the original design, and the appearance of the bridge body shows no significant differences; for example, it maintains the fundamental form of 3 × 3. In addition, the foundation depth is similar to that of the original design. Relatively speaking, only the dimensions of the piers show a significant difference (Table 11). The primary reason for this is that the original bridge structure has recently been modified for reinforcement, and its failure probability already approaches the target value assumed in this study; consequently, the RBDO result and the dimensions of the original bridge have not changed significantly. Note that the RBDO suggests decreasing the diameter of the pier and increasing the depth, which indicates that the design of the original bridge pier was overly conservative in terms of the water flow rate and the water level at the location of the bridge. Therefore, reducing the bridge pier dimensions is suggested to reduce the volume. Note that this study only examined the ability of the bridge to resist floods; impacts caused by earthquakes have not been taken into consideration.

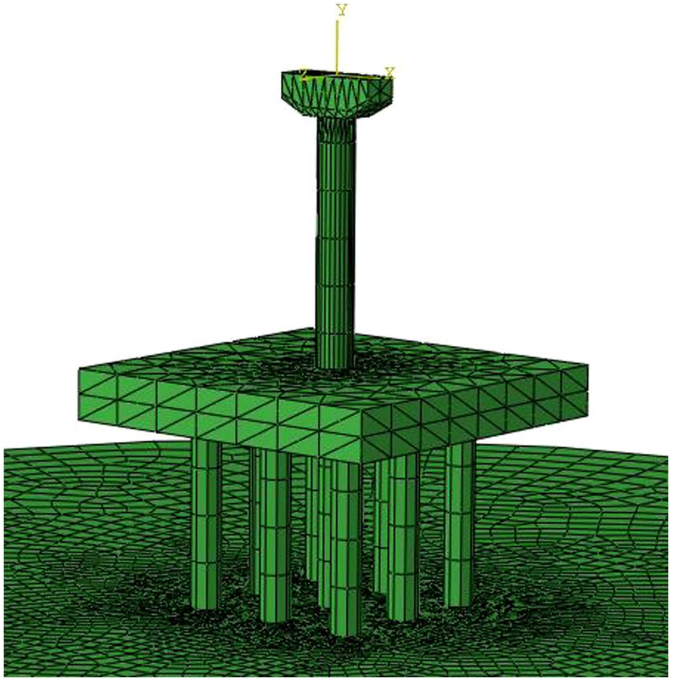

Fig. 7. Finite-element model of optimal design via RBDO

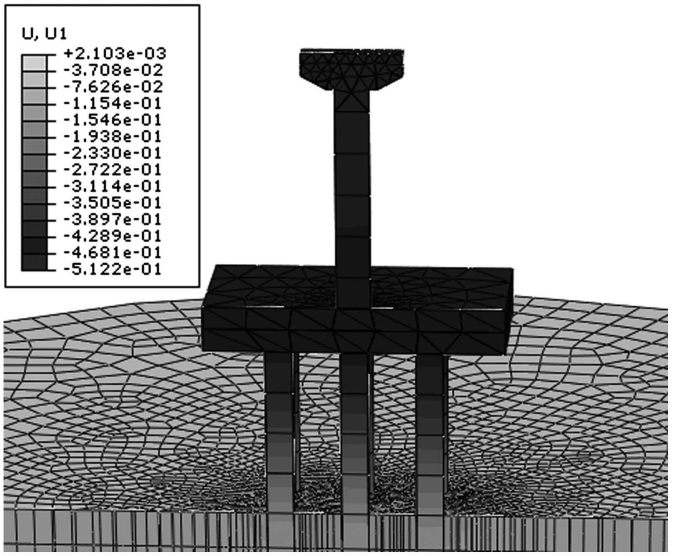

Fig. 8. Displacement distribution graph of optimized bridge (units: centimeters)

Table 11. Results of RBDO

Bridge components and statistics	Dongshi Bridge	RBDO result
Pier diameter (m)	2.60	1.50
Pier height (m)	8.00	10.00
Pile cap thickness (m)	2.50	2.05
Pile diameter (m)	1.50	1.35
Pile depth (m)	20.00	21.15
Pile type	3 × 3	3 × 3
Total volume (m^3)	5.49×10^2	4.35×10^2
Percentage of volume reduction	0.2077	0.2077

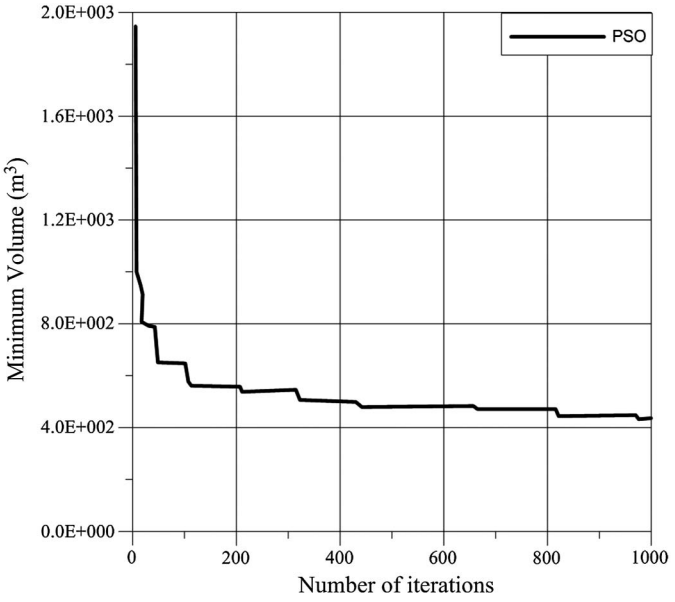

Fig. 9. Convergence history of PSO

2. Regarding the convergence condition of the particle group algorithm, Fig. 9 shows the convergence history of the PSO. The optimization was performed on a computer equipped with Core i7, CPU@3.4 GHz, and 10GB RAM. The convergence was fast and stable, capable of approaching a constant value within 100 iterations in approximately 600 s.
3. The failure mode of the bridge system is primarily controlled by the pile head displacement (Table 12), and the failure probability of the optimized bridge is slightly higher than that of the original designed bridge. The reliability index of the original bridge is approximately 3.1, which is greater than the target reliability ($\beta = 3.0$). Therefore, during the optimization, there is room to adjust the volume, and the optimized total volume is approximately four-fifths of the original bridge for a failure rate within the tolerance range.
4. Regarding the accuracy verification of RSM, Table 13 shows that among the five limit states, the RSMs of the soil bearing and the pile head displacement show relatively better accuracy, whereas the other three RSMs can still be improved. However, because the last three limit state functions do not contribute to the system's reliability, they have no significant influence on the optimization result. Consequently, the following only provides further investigation into the soil bearing and the pile head displacement.

Fig. 10 shows a relationship diagram for the foundation pile diameter and the depth and soil bearing reliability index, which includes various basic designs (e.g., 3×3 and 4×4), and the relationships are not clear. Figs. 11 and 12 describe the impacts of diameter and depth, respectively, on the soil bearing reliability index. Based on Fig. 11, pile diameter has no obvious impact on the soil bearing reliability index. However, based on Fig. 12, pile depth and soil bearing capacity show an approximately linear relationship

Table 13. Accuracy Evaluation of RSM Models

Failure mode	Soil bearing	Pile axial stress	Pile shear stress	Soil pulling force	Pile head displacement
R^2	0.99	0.41	0.61	0.62	0.95
MAPE	3.64	88.27	23.41	61.67	13.14
RMSE	0.18	24.50	12.88	4.48	0.64

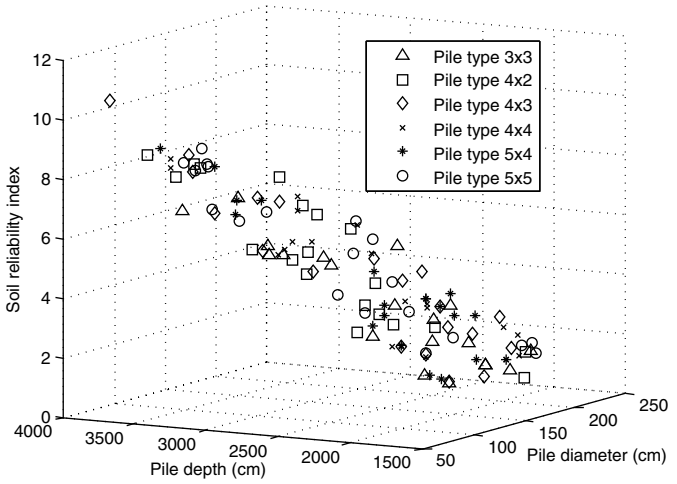

Fig. 10. Relationship among pile diameter, depth, and soil bearing reliability index

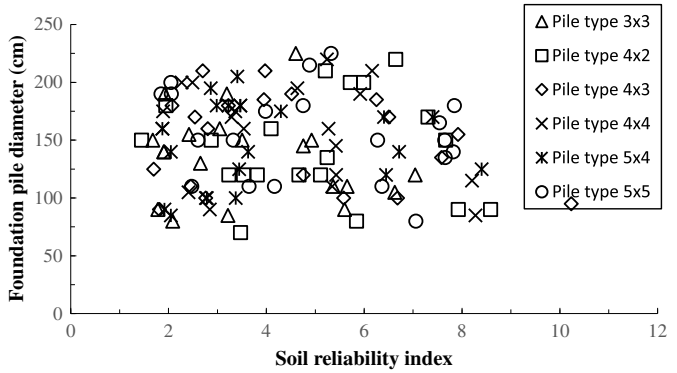

Fig. 11. Relationship between pile diameter and soil bearing reliability index

such that the greater the depth, the higher the reliability index, which is a logical trend. Fig. 13 only includes the basic type, 3×3, and the impact of pile depth on the soil bearing reliability index is clear. It is difficult to reach a conclusion regarding a relationship between pile diameter and the soil bearing reliability index. As for the relationships between pile diameter, depth, and pile head displacement reliability index, as shown in Figs. 14–17, it can be seen that, as opposed to soil bearing, pile top displacement is

Table 12. Failure Probability (P_f) for Each Failure Mode

Failure mode	Soil bearing	Pile axial stress	Pile shear stress	Soil pulling force	Pile head displacement
P_f of the existing Dongshi Bridge (FOSM)	~0	~0	~0	~0	9.6×10^{-4}
P_f of the optimized Dongshi Bridge (RSM)	5×10^{-4}	~0	~0	~0	1.1×10^{-3}
P_f of the optimized Dongshi Bridge (FOSM)	8.5×10^{-6}	~0	~0	~0	9.0×10^{-4}

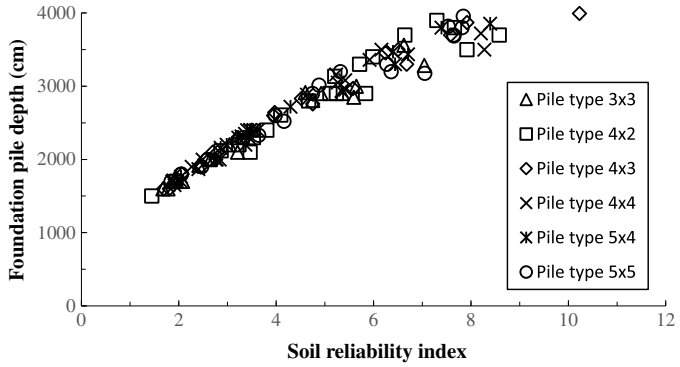

Fig. 12. Relationship between pile depth and soil bearing reliability index

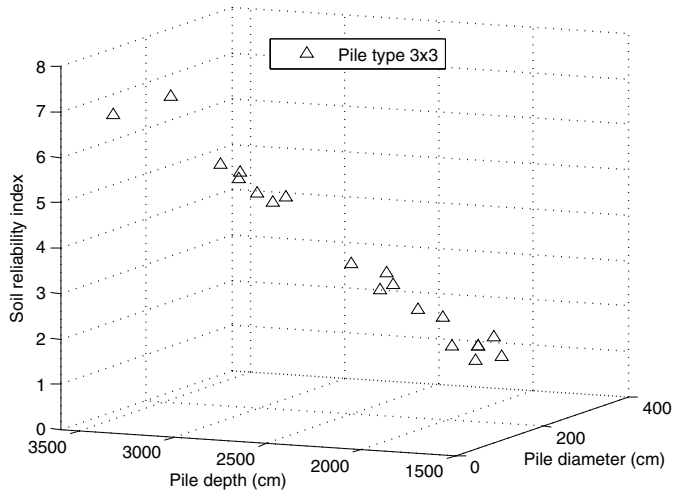

Fig. 13. Relationship among pile diameter, depth, and soil bearing reliability index (using basic 3×3 type as example)

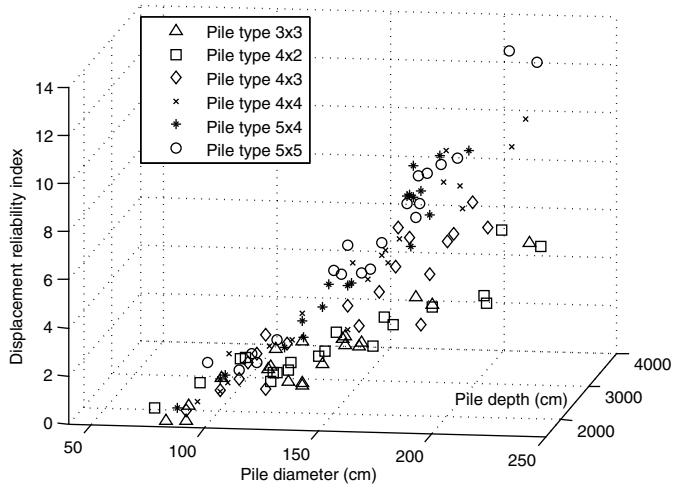

Fig. 14. Relationship among pile diameter, depth, and pile head displacement reliability index

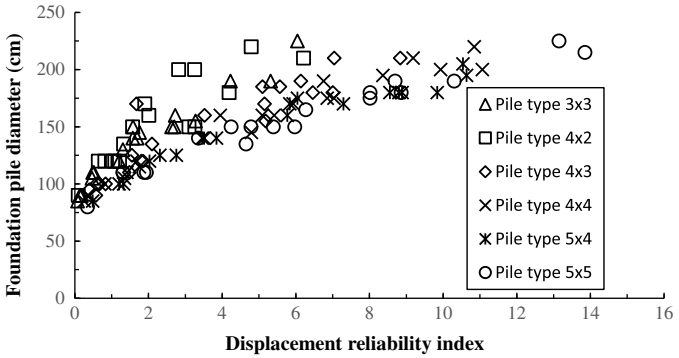

Fig. 15. Relationship between pile diameter and pile head displacement reliability index

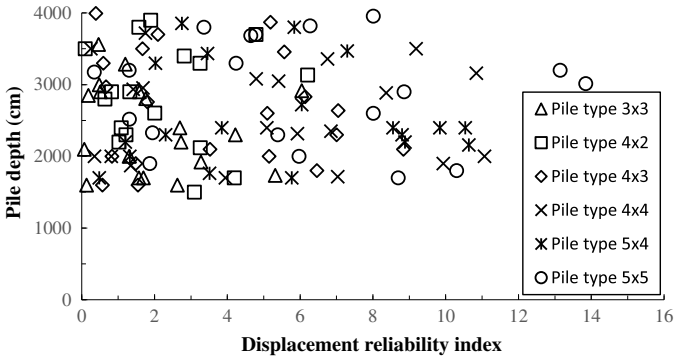

Fig. 16. Relationship between pile depth and pile head displacement reliability index

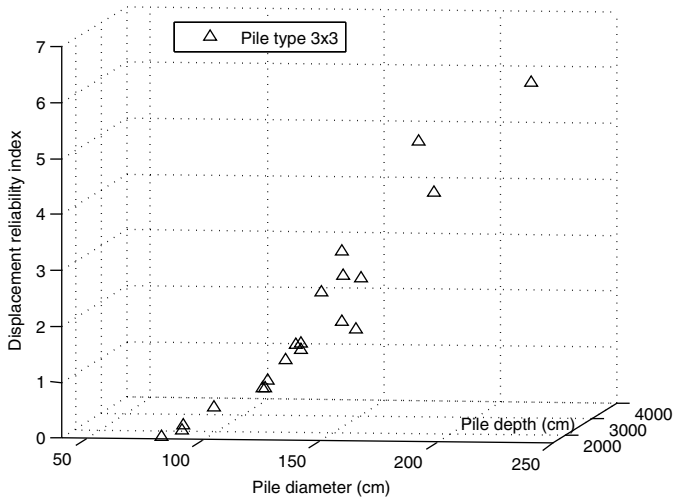

Fig. 17. Relationship among pile diameter, depth, and pile head displacement reliability index (using basic 3×3 type as example)

primarily affected by pile diameter (Fig. 15). According to Table 13, two of the primary limit state functions have relatively higher accuracy. In addition, the trends predicted by the surrogate model are consistent with the analytical equations. Even though there are still some errors in the result, all the trends of the surrogate model were conservative. Therefore, the use of the surrogate model to perform reliability-based optimization on river bridges is considered feasible.

Conclusions

The safety of river bridges is an important issue in Taiwan. Because many uncertainties are involved in the evaluation process, this study proposes a reliability optimization design algorithm to ensure bridge safety not only in the analysis phase but also in the design phase. The proposed algorithm uses LHS to allocate the sample points. For each sample, FOSM is used to calculate the reliability index. Based on the results of FOSM, LS-SVM is used to construct the response surface. According to the constructed response surface, PSO is used to perform the reliability-based optimization. In addition, to increase the accuracy of the deterministic model, three-dimensional finite-element software is used to perform structural analysis and the Python programming language is used to build an automatic computation structure, in which the uncertainty of the random variables is constructed via a hydraulic analysis. Only the flood resistance ability of the bridge was considered here. The influence of earthquakes was not considered. According to the results of the analysis, several conclusions can be drawn.

1. Under the premise of satisfying the safety requirements, there is still room for improvement in the current design against floods; for example, the optimal values of the pier dimension, pile cap, and pile diameter are all smaller than the original design values, and the pile depth should be increased.
2. With the automatic computation structure constructed by Python, the computation efficiency of the reliability analysis and optimization design can be effectively increased.
3. The 120 samples generated by LHS were used by LS-SVM to construct five failure modes for the surrogate model. The result indicates that the predictions of the nonprimary controlled failure mode are relatively poor, whereas the predictions of the primary controlled failure modes are relatively strong.
4. The predicted trends of the proposed finite-element analysis are consistent with the conventional engineering determinations, indicating that the proposed calculation details of the numerical model are suitable.
5. During the optimization process, six types of piles were considered, all of which were geometrically symmetrical. An actual engineering design may be different due to onsite field factors, and the six types currently considered may be insufficient in practice.

Acknowledgments

This study was supported by the National Science Council of Taiwan under Grant No. NSC 102-2221-E-011-078-MY2. The support is gratefully acknowledged.

References

ABAQUS [Computer software]. Dassault Systèmes, Waltham, MA.

ACE/HEC (Army Corps of Engineers and Hydrologic Engineering Center). (1997). *HEC-RAS, river analysis system, hydraulic reference manual*, Davis, CA.

Aoues, Y., and Chateauneuf, A. (2010). "Benchmark study of numerical methods for reliability-based design optimization." *Struct Multidiscip. Optim.*, 41(2), 277–294.

Chang, Y. L., and Chou, N. S. (1989). "Chang's simple side pile analysis approach." *Sino-Geotech.*, 25, 64–82.

Cortes, C., and Vapnik, V. (1995). "Support-vector networks." *Mach. Learn.*, 20(3), 273–297.

Eberhart, R. C., and Kennedy, J. (1995). "A new optimizer using particle swarm theory." *Proc., IEEE Int. Symp. on Micro Machine and Human Science*, IEEE, New York, 39–43.

Fu, S. L. (2012). "Analysis for laterally loaded test of the caisson foundation at Nioudou Bridge." Master thesis, National Taiwan Univ., Taipei City, Taiwan, 48–51.

Ho-Hsien Engineering and Technology Consultants. (2011). "Geological drilling report for Dajia River." *Proc., Drilling Rep.*, Ho-Hsien Engineering and Technology Consultants, Taichung City, Taiwan, 3–1.

Kaymaz, I., and Marti, K. (2007). "Reliability-based design optimization for elastoplastic mechanical structures." *Comput. Struct.*, 85(10), 615–625.

Kennedy, J., and Eberhart, R. C. (1995). "Particle swarm optimization." *Proc., IEEE Int. Conf. on Neural Networks*, IEEE, New York, Vol. 4, 1942–1948.

Ko, Y. Y., Chiou, J. S., Tsai, Y. C., Chen, C. H., Wang, H. W., and Wang, C. Y. (2014). "Evaluation of flood-resistant capacity of scoured bridges." *J. Perform. Constr. Facil.*, 10.1061/(ASCE)CF.1943-5509.0000381, 61–75.

Li, F., Wu, T., Hu, M., and Dong, J. (2010). "An accurate penalty-based approach for reliability-based design optimization." *Res. Eng. Des.*, 21(2), 87–98.

Liang, J. H., Mourelatos, Z. P., and Nikolaidis, E. (2007). "A single-loop approach for system reliability-based design optimization." *J. Mech. Des.*, 129(12), 1215–1224.

Liao, K. W., and Lu, H. (2012). "A stability investigation of a simulation- and reliability-based optimization." *Struct Multidiscip. Optim.*, 46(5), 761–781.

Liao, K. W., Lu, H. J., and Wang, C. Y. (2015). "A probabilistic evaluation of pier-scour potential in the Gaoping River Basin of Taiwan." *J. Civ. Eng. Manage.*, 21(5), 637–653.

Liao, K. W., Muto, Y., Chen, W. L., and Wu, B. H. (2016). "A probabilistic bridge safety evaluation against floods." *SpringerPlus*, 5(783), 1–19.

Lin, C., Bennett, C., Han, J., and Parsons, R. (2015). "Effect of soil stress history on scour evaluation of pile-supported bridges." *J. Perform. Constr. Facil.*, 10.1061/(ASCE)CF.1943-5509.0000681, 04014178.

Motta, R. S., and Afonso, S. M. B. (2016). "An efficient procedure for structural reliability-based robust design optimization." *Struct. Multidiscip. Optim.*, 54(3), 511–530.

NCDR (National Science and Technology Center for Disaster Reduction). (2010). "Disaster survey and analysis of Morakot typhoon." *Proc., Morakot Typhoon Survey Rep.*, National Science and Technology Center for Disaster Reduction, Taipei, Taiwan, 347.

Ni, S.-H., Huang, Y. H., and Lo, K. F. (2012). "Numerical investigation of the scouring effect on the lateral response of piles in sand." *J. Perform. Constr. Facil.*, 10.1061/(ASCE)CF.1943-5509.0000224, 320–325.

Pan, G. L. (2007). *General principle on engineering geology*, Wu-nan Books, Taipei, Taiwan, 244.

Shan, S., and Wang, G. G. (2008). "Reliable design space and complete single-loop reliability-based design optimization." *Reliab. Eng. Syst. Saf.*, 93(8), 1218–1230.

Suykens, J. A. K., Gestel, T. V., Brabanter, J. D., Moor, B. D., and Vandewalle, J. (2002). *Least squares support vector machines*, World Scientific, Singapore, 71–76.

Wardhana, K., and Hadipriono, F. C. (2003). "Analysis of recent bridge failures in the United States." *J. Perform. Constr. Facil.*, 10.1061/(ASCE)0887-3828(2003)17:3(144), 144–150.